The Use of FDG-PET in the Detection and Management of Malignant Lymphoma: Correlation of Uptake with Prognosis

Junichi Okada, Kyosan Yoshikawa, Keiko Imazeki, Satoshi Minoshima, Kimiichi Uno, Jun Itami, Junpei Kuyama, Hirotaka Maruno, and Noboru Arimizu

Department of Radiology, Chiba University, School of Medicine, Chiba, Japan

Twenty-one patients with untreated malignant lymphoma in the head and neck region were evaluated with positron emission tomography (PET) using fluorine-18-fluorodeoxyglucose (FDG) and gallium-67 SPECT imaging. Tumor-to-normal soft-tissue contrast ratios (TCRs) obtained 60 min after injection of FDG were higher than 2.6, and all malignant lymphomas were clearly visualized. In patients with poor prognosis, higher TCRs and glucose utilization rates (GURs) were observed, whereas low TCR and GUR were shown in a patient with low-grade malignancy. In comparison with ^{67}Ga scintigraphy, patients with high TCRs and GURs were likely to show increased accumulation of gallium-67, but accumulation of gallium-67 was not increased as much as FDG in poor prognostic patients. FDG-PET may be useful in the detection and management of malignant lymphoma.

J Nucl Med 1991;32:686–691

Gallium-67 (^{67}Ga) has been employed in the diagnosis, staging, and treatment of malignant lymphoma, but its role in the management of these patients is controversial (*1–3*). Gallium-67 is difficult to analyze quantitatively and suffers from low spatial resolution.

Positron emission tomography (PET) using fluorine-18-2-deoxy-2-fluoro-D-glucose (FDG) has been used to measure regional glucose metabolism in oncology. Tumors are usually visualized as areas of increased FDG accumulation. Elevated metabolic states have been observed in more aggressive tumors (*4–8*). Several investigators have concluded that FDG is a useful imaging agent in malignant tumors.

In this study, FDG-PET techniques were performed, and compared with ^{67}Ga scintigraphy. Correlations between these two imaging modalities and these patients' pathologic diagnoses, tumor size, and prognoses were made to evaluate the usefulness of PET-FDG techniques in the detection and management of these neoplasms.

Received Mar. 1, 1990; revision accepted Sept. 12, 1990.

For reprints contact: Junichi Okada, MD, Department of Radiology, Chiba University, School of Medicine, 1-8-1 Inohana, Chiba City, 280 Japan.

MATERIALS AND METHODS

Twenty-one adult patients between the ages of 37 and 86, with untreated malignant lymphoma in the head and neck region were studied (Table 1). The patients were followed for longer than 6 mo after treatment. One patient with low-grade non-Hodgkin's lymphoma (Case 1) required radiotherapy, and disease progression was not observed after 12 mo. In 13 patients with intermediate-grade non-Hodgkin's lymphoma and in two patients with Hodgkin's disease, complete clinical remission was obtained with therapy within 3 mo. In three patients with intermediate-grade non-Hodgkin's lymphoma (Cases 10, 11, and 16), complete remission (CR) was not obtained and death occurred within 4 mo after treatment. In one patient with intermediate-grade non-Hodgkin's lymphoma (Case 14), remission was obtained, but relapses occurred outside the cervical region. In one patient with high grade non-Hodgkin's lymphoma (Case 19), remission was obtained, but a disseminated intravascular coagulation, whose cause could not be conclusively proved but may have been associated with an infection and a relapse of lymphoma, followed and the patient died.

In all patients, the tumors were diagnosed in Working Formulation for clinical usage, and divided into low-, intermediate-, and high-grade neoplasms (*9*). Tumor size was measured on a transaxial image of x-ray computerized tomography (CT) or magnetic resonance imaging (MRI) in which the tumor was shown at maximum size.

FDG was synthesized by CYPRIS and CUPID, a cyclotron system at our institute made by Sumitomo Heavy Industry, About 4 mCi (148 MBq) of FDG were injected intravenously with the patients in a fasting state. Arterial blood samples were drawn to monitor the plasma concentration of FDG and glucose.

A series of 2-min sequential scans (dynamic scans) were acquired with a Shimazu-SET130W PET scanner for 60 min after injection. Three slices were acquired simultaneously with a slice thickness of 1.65 cm and an inplane spatial resolution of 1.04 cm FWHM. Patients were positioned to obtain PET images on the plane in which the tumors were shown at maximum size on x-ray CT or MRI.

The tumor activity of FDG on the reconstructed transaxial images increased continuously for 60 min in all patients. Tumor-to-normal soft-tissue contrast ratios (TCRs) were measured by using 10 mm x 10 mm square regions of interest (ROIs). A tumor ROI was placed on an area where the accumulation of FDG was highest in tumor. A normal soft-tissue ROI was placed in soft tissue consisting mainly of paravertebral musculature around the vertebral bone.

TABLE 1
Clinical and Histologic Findings

Case	Age	Sex	Diagnosis*	Grading	Tumor size (mm)	Treatment†	Outcome‡
1	56	M	Non-Hodgkin small, lympho	Low	53 × 18	Chemo RT	NR
2	63	F	Non-Hodgkin diffuse, mixed	Intermediate	37 × 11	Chemo RT	CR
3	56	F	Non-Hodgkin diffuse, mixed	Intermediate	35 × 35	RT	CR
4	77	F	Non-Hodgkin diffuse, mixed	Intermediate	36 × 18	Chemo RT	CR
5	54	M	Non-Hodgkin diffuse, mixed	Intermediate	50 × 21	Chemo RT	CR
6	51	M	Non-Hodgkin diffuse, mixed	Intermediate	28 × 17	Chemo	CR
7	50	M	Non-Hodgkin diffuse, large	Intermediate	44 × 21	RT	CR
8	43	F	Non-Hodgkin diffuse, large	Intermediate	37 × 16	Chemo RT	CR
9	66	M	Non-Hodgkin diffuse, large	Intermediate	26 × 7.5	RT	CR
10	85	M	Non-Hodgkin diffuse, large	Intermediate	61 × 61	Chemo	PR died
11	84	M	Non-Hodgkin diffuse, large	Intermediate	75 × 36	Chemo	PR died
12	42	M	Non-Hodgkin diffuse, large	Intermediate	25 × 25	Chemo	CR
13	77	M	Non-Hodgkin diffuse, large	Intermediate	48 × 24	Chemo RT	CR
14	84	M	Non-Hodgkin diffuse, large	Intermediate	50 × 24	RT	CR relapsed
15	63	M	Non-Hodgkin diffuse, large	Intermediate	53 × 34	RT	CR
16	78	M	Non-Hodgkin diffuse, large	Intermediate	44 × 22	Chemo	PR died
17	60	F	Non-Hodgkin follic., large	Intermediate	30 × 12	Chemo RT	CR
18	69	M	Non-Hodgkin diffuse, small	Intermediate	71 × 62	RT	CR
19	49	M	Non-Hodgkin immunoblastic	High grade	32 × 25	Chemo	CR, DIC died
20	35	M	Hodgkin		38 × 18	RT	CR
21	39	M	Hodgkin		53 × 24	RT	CR

* Diagnosis classified by the Working Formulation. Small, lympho = small lymphocytic; diffuse, mixed = diffuse, mixed small, and large cell; diffuse, large = diffuse, large cell; follic., large = follicular large cell; diffuse, small = diffuse small-cleaved cell; and immunoblastic = large cell, immunoblastic.

† Chemo = chemotherapy and RT = radiotherapy.

‡ NR = no response; CR = complete response; PR = partial response; and DIC = disseminated intravascular coagulation.

The glucose utilization rate (GUR) was calculated using the graphic method demonstrated by Patlak and by Gjedde et al. This method uses sequential measurements of multiple uptake data by setting 10 mm x 10 mm square ROIs on the tumor. Figure 1 shows a graph of the distribution coefficient $Ci^*(t)/C^*p(t)$ versus virtual time $\int_0^t Cp^*(t')dt'/Cp^*(t)$. The slope of the linear part of this plot represents k1k3/(k2+k3). The metabolic rate of glucose was calculated by Cpk1k3/LC(k2+k3) (*10–12*) in 20 patients. For the lumped constant (LC), we adopted the value of 0.52 measured by Reivich et al. (*13*) to obtain a rough estimate of GURs.

Gallium-67 imaging was performed 72 hr after intravenous injection of 4 mCi of ^{67}Ga-citrate. The conventional planar images, acquired with a Toshiba GCA 401-5 gamma camera, were graded by visual inspection in all patients as follows:

- − : difficult to visualize the tumor without other localizing information.
- + : possible to visualize the tumor without other localizing information.
- ++ : easily visualized; ^{67}Ga accumulation exceeded that of the skull.

Single-photon emission tomography (SPECT) using ^{67}Ga was performed with the Shimazu-SCINTIPAK-2400 system in seven patients. Scan data were acquired by 64 projections in a 360°

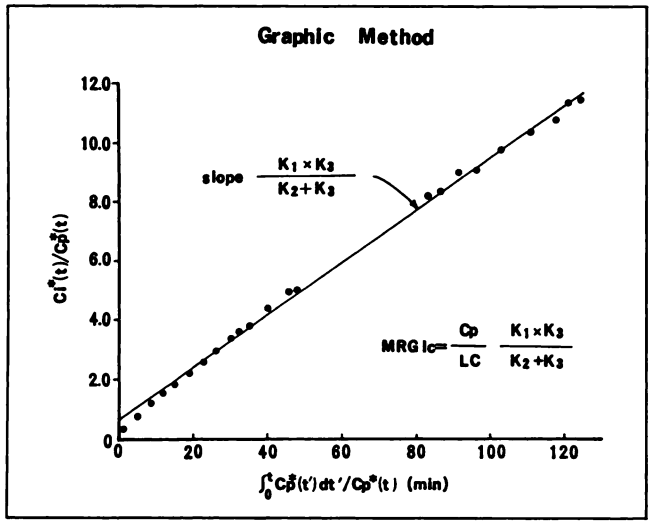

FIGURE 1. Graph of the distribution coefficient Ci*(t)/Cp*(t) versus $\int_0^t Cp^*(t')dt'/Cp^*(t)$. In this graphic approach, the slope of the linear part represents k1k2/(k2+k3) and the metabolic rate of glucose can be derived from this slope.

orbit at a rate of 30 sec per projection. The collected data was reconstructed with a Butterworth filter and RPC attenuation correction algorithm (*14*). In this SPECT system, the inplane spatial resolution was 2.3 cm FWHM. TCRs were calculated by setting the ROI on the transaxial images in a similar fashion to setting used in the PET study. For ^{67}Ga imaging, a medium-energy collimator and twenty percent windows centered over the 93 and 184 keV photon peaks were used.

RESULTS

Mean values of tumor sizes, TCRs, and GURs were shown in Table 2, and the relationship between tumor size and TCR on PET images is shown in Figure 2. TCRs of all tumors were greater than 2.6 from a patient with low-grade non-Hodgkin's lymphoma (Fig. 3), and all tumors were clearly visualized as hot spots on his PET images. In three cases of intermediate-grade non-Hodgkin's lymphoma in which complete remission could not be obtained and in the patient with high-grade non-Hodgkin's lymphoma, high TCRs were demonstrated (Fig. 4). The relationship between tumor size and TCR was not significant (r = 0.318).

In all patients, GURs of normal soft tissue were less than 1.15 mg/100 g/min. Increased GURs were demonstrated in all tumors (Fig. 5), but were especially high in three patients with intermediate grade non-Hodgkin's lymphoma with poor prognosis and in the patient with high-grade non-Hodgkin's lymphoma. The lowest GUR was observed in the patient with low-grade non-Hodgkin's lymphoma. The relationship between tumor size and GUR was not significant (r = 0.339).

One intermediate-grade patient, in whom remission was obtained but relapses followed, showed few differences of TCR and GUR from intermediate-grade patients without

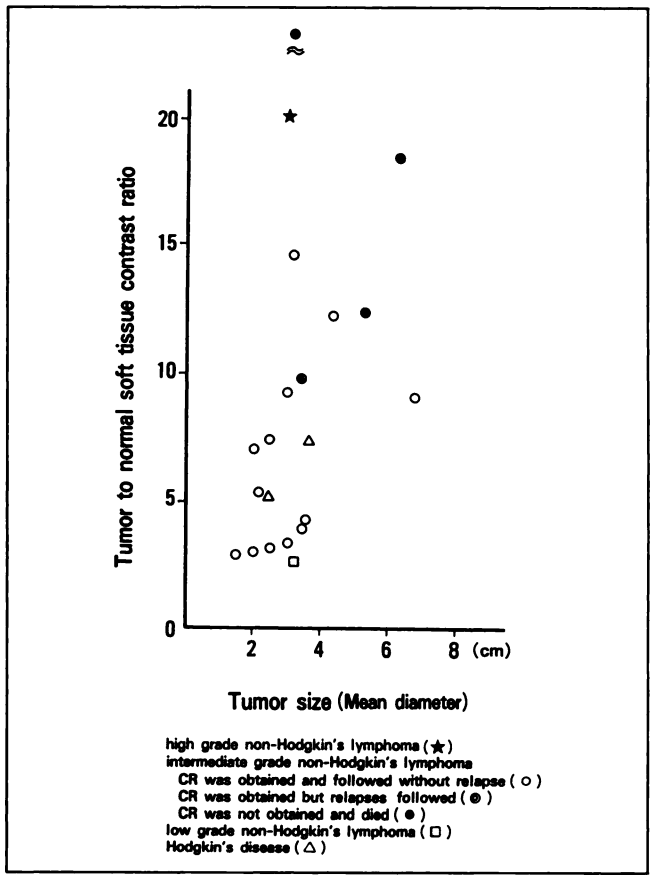

FIGURE 2. Plot of TCRs on PET images versus tumor sizes. TCRs were increased in a patient with high-grade non-Hodgkin's lymphoma (★) and three patients with intermediate-grade non-Hodgkin's lymphoma with poor prognosis (●), whereas TCR of a low-grade non-Hodgkin's lymphoma (□) was lowest.

TABLE 2
Mean Values of Tumor Sizes, TCRs, and GURs

	n	Tumor size (cm)	TCR	GUR (mg/100 g/min)
High-grade non-Hodgkin's lymphoma (★)	1	2.8	20.3	15.9
Intermediate-grade non-Hodgkin's lymphoma				
CR was not obtained and died (●)	3	4.8 ± 1.5	22.0 ± 11.7	21.5 ± 8.8
CR was obtained but relapses followed (◉)	1	3.5	9.93	6.65
CR was obtained and relapses were not found (○)	13	3.0 ± 1.3	6.59 ± 3.85	5.86 ± 2.6
Low-grade non-Hodgkin's lymphoma (■)	1	3.1	2.61	1.59
Hodgkin's disease (△)	2	2.9 ± 0.9	6.24 ± 1.6	4.92 ± 1.22

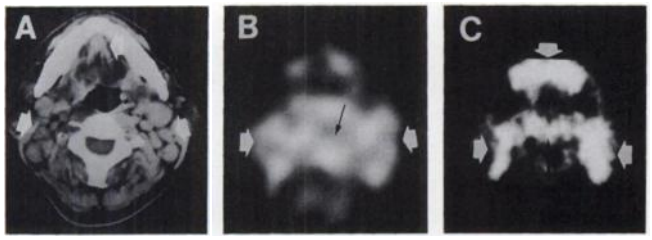

FIGURE 3. Case 1: non-Hodgkin's, small lymphocytic lymphoma (low-grade). (A) The CT scan shows tumors of the submental and bilateral jugular lymph nodal area (white arrow). (B) In the SPECT image using ^{67}Ga, increased accumulation of ^{67}Ga was observed in the tumor (white arrow) and vertebral bone (black arrow). (C) In the PET image, tumors were demonstrated as hot spots of FDG (white arrow) and TCR was 2.6. Increased activity of FDG was also observed in normal pharyngeal mucosa (black arrow).

recurrences of the tumor. Though the number of patients with Hodgkin's disease was limited, the differences of TCRs and GURs between non-Hodgkin's lymphoma and Hodgkin's disease were not significant.

Plots of GURs versus visual grading of ^{67}Ga planar images are shown in Figure 6. In a patient with an intermediate-grade non-Hodgkin's lymphoma, it was difficult to point out a tumor, measuring 2.5 x 0.8 cm, on the planar ^{67}Ga image. On the other hand, this tumor was clearly visualized on the PET image (Fig. 7). In patients with high GURs, increased accumulation of ^{67}Ga was observed, but the relationships between GUR and accumulation of ^{67}Ga were not significant ($r = 0.374$). The comparison between TCR in PET using FDG and that in SPECT using ^{67}Ga is shown in Figure 8. Patients with high TCRs on PET-FDG were likely to show increased uptake of ^{67}Ga, but the relationship was not significant ($r = 0.359$). Gallium-67 accumulation was not increased as much as FDG in the high-grade patient and in the intermediate-grade patients with poor prognosis.

DISCUSSION

The use of PET-FDG in oncology has primarily concentrated on brain tumors. In some articles, glucose metabolic

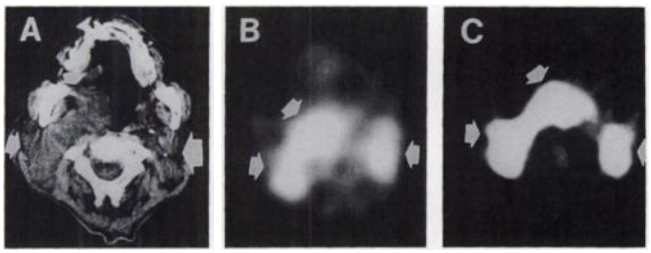

FIGURE 4. Case 11: non-Hodgkin's, diffuse large lymphoma (intermediate grade) with poor prognosis. (A) The CT scan shows tumors of the right parapharyngeal, right jugular, and left jugular area (white arrow). In the SPECT (B) and the PET (C) images, the tumors were demonstrated as increased activity (white arrow) and TCR in PET was 12.4.

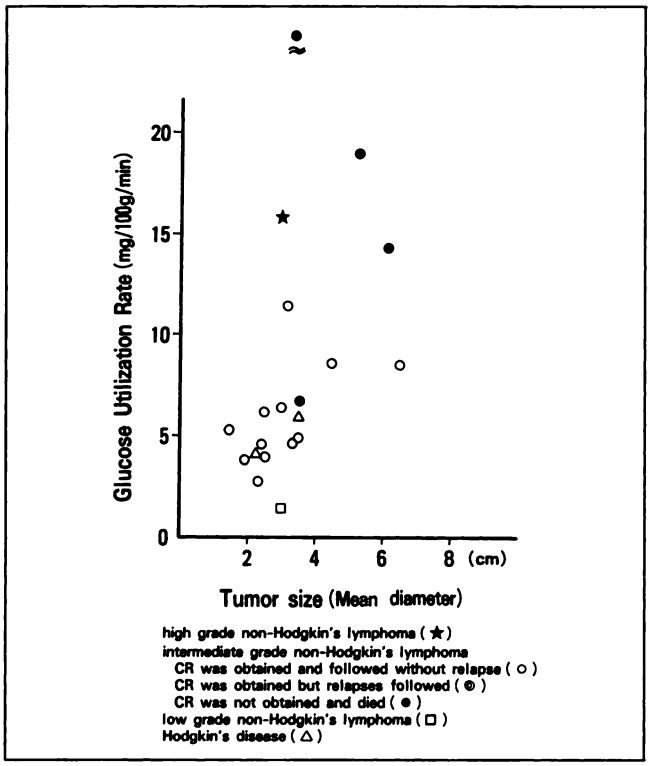

FIGURE 5. Plot of glucose utilization rates versus tumor sizes. Tumors of a high-grade non-Hodgkin's lymphoma (★) and three intermediate-grade non-Hodgkin's lymphomas with poor prognosis (●) showed high GURs. A low-grade non-Hodgkin's lymphoma (□) showed the lowest GUR.

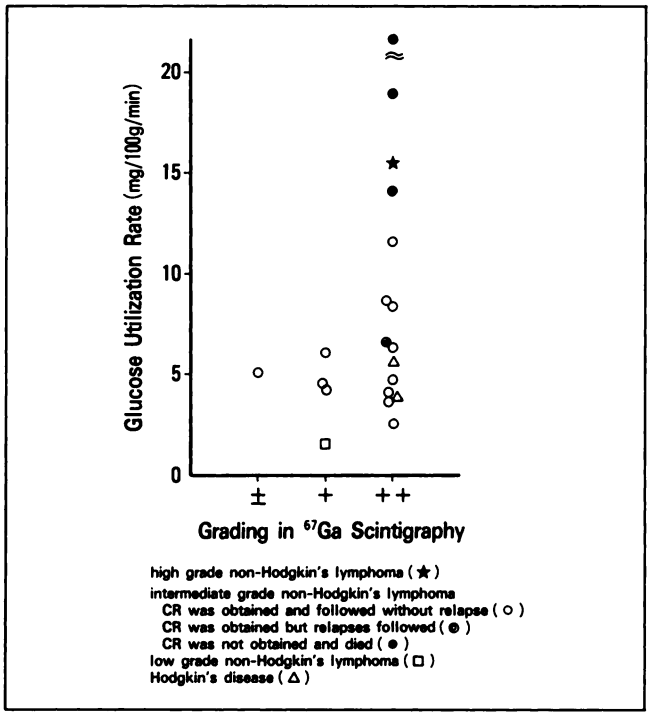

FIGURE 6. Plot of glucose utilization rates versus visual grading of ^{67}Ga planar image. In patients with high TCRs and glucose utilization rates, increased accumulation of ^{67}Ga was observed.

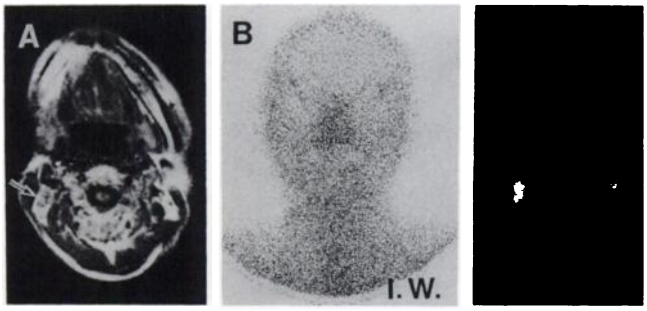

FIGURE 7. Case 9: non-Hodgkin's, diffuse large lymphoma (intermediate-grade). (A) MRI shows the swelling of right jugular lymph nodes (black arrow). It was difficult to point out the tumor on the ^{67}Ga planar image (B). On the PET image (C), the increased activity of the tumor was clearly visualized (white arrow). The accumulation of FDG was also increased in normal left parotid gland (black arrow head).

rates correlated with the aggressiveness of brain tumors and were useful for prognosis of patients with gliomas and meningiomas (*5,7*). In the evaluation of hepatic and musculoskeletal tumors, FDG accumulation correlated with pathologic gradient (*4,8*). In malignant lymphoma, ^{67}Ga scintigraphy has been employed for detection of tumors, but its value in clinical practice is controversial because of limitations of spatial resolution, sensitivity, and quantitative analysis (*1–3*). FDG was reported to be more sensitive than ^{67}Ga for detecting non-Hodgkin's lymphoma on

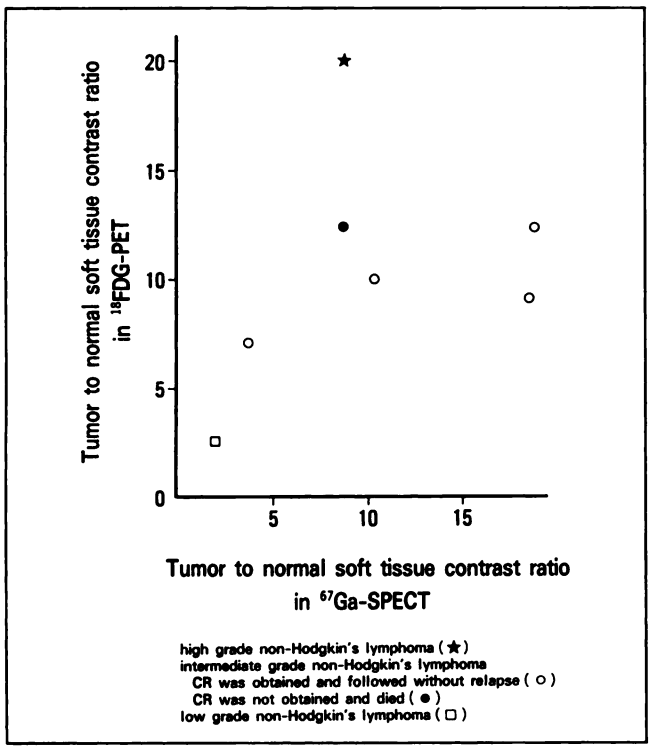

FIGURE 8. Plot of TCR in FDG-PET versus TCR in ^{67}Ga-SPECT. Patients with high TCRs on PET-FDG were likely to show increased uptake of ^{67}Ga, but accumulation of ^{67}Ga was not increased as much as FDG in the high-grade patient (★) and the intermediate-grade patients with poor prognosis (●).

planar images in five patients (*6*). We applied PET-FDG in 21 untreated patients with lymphomas to study usefulness for the detection and management of malignant lymphoma.

TCRs on PET images were greater than 2.6, and tumors in all patients were clearly visualized 60 min after injection. The lowest TCR occurred in a patient with a low-grade, small lymphocytic lymphoma. Most of these neoplasms have low mitotic rates and patients tend to survive despite persistent disease (*15*). On the other hand, a high TCR was observed in a patient with a high-grade immunoblastic lymphoma, a very aggressive neoplasm which is associated with a short period of survival when intensive therapy is not applied (*15*). High TCRs were also observed in three intermediate-grade patients with poor prognosis in whom remissions were not obtained.

The relationship between tumor size and TCR was not significant. In our PET system, the recovery coefficient (RC) (*16*) caused by the partial volume artifact was measured by the use of a spherical phantom. When the diameter of the phantom was 20 mm, 30 mm and 40 mm, RC by using 10 x 10 mm square ROI was 0.64, 0.93, and 0.99, respectively (*17*). A TCR and a GUR of a tumor whose size was smaller than 40 mm could be increased, if the partial volume artifact could be excluded. And the coefficient of the relationship between tumor size and TCR could be decreased. The relationship between tumor size and GUR was not significant, either. FDG-PET is believed to offer information that cannot be acquired by a study of tumor size.

To measure GUR, we used the graphic method proposed by Patlak and Gjedde et al. (*10–12*). If FDG enters a second tissue distribution region, which in this study is a malignant lymphoma and is unable to exit once inside, a GUR can be easily obtained without knowledge of individual rate constants. In tumors, activity of glucose-6-phosphatase was reported to be low and intracellular trapping of FDG was observed (*18,19*). Though the LC of each tumor is unknown and may be significantly different, we applied this graphic method by adopting the lumped constant as 0.52, which was reported in normal brain tissue by Reivich et al. (*13*), to obtain a rough estimate of GUR in malignant lymphoma. GUR of malignant lymphoma was greater than that of normal soft tissue. The distribution tendency of GUR was similar to that of TCR, and patients in whom remissions could not be obtained and poor prognosis followed showed high TCRs and GURs.

We compared PET using FDG with the ^{67}Ga planar image and the SPECT image. Tumors of twenty patients were detected on the ^{67}Ga images, but one, measuring 2.6 x 0.8 cm, was not easily detected. On the other hand, all tumors were visualized on FDG-PET. In seven cases, tumors were evaluated on both PET and SPECT images. PET is expected to yield better quantitative results in addition to exceptional contrast with greater spatial reso-

lution than SPECT (*20*). Cases with high TCRs in PET were likely to show increased uptake of ^{67}Ga, but accumulation of ^{67}Ga was not increased as much as that of FDG in patients with poor prognosis. Studies in which accumulation of ^{67}Ga were evaluated according to pathologic grading and prognosis in malignant lymphoma are not satisfactory, due to the limitation of quantitative analysis and the uncertainty concerning how ^{67}Ga is accumulated (*21–23*). On the other hand, better correspondence between the metabolic state of FDG and the prognosis was demonstrated compared with ^{67}Ga. Our results suggest that FDG-PET may be useful as a method both for detecting malignant lymphoma and for predicting the response to therapy and the prognosis.

REFERENCES

1. Rudders R, McCaffrey JA, Kahn PC. The relative roles of gallium-67-citrate scanning and lymphangiography in the current management of malignant lymphoma. *Cancer* 1977;40:1439–1443.
2. Longo DL, Schilsky RL, Blei L, et al. Gallium-67 scanning: limited usefulness in staging patients with non-Hodgkin's lymphoma. *Am J Med* 1980;68:695–700.
3. Tumeh SS, Rosenthal DS, Kaplan WD, et al. Lymphoma: evaluation with Ga-67 SPECT. *Radiology* 1987;164:111–114.
4. Yonekura Y, Benua RS, Brill P, et al. Increased accumulation of 2-deoxy-2-[^{18}F]fluoro-D-glucose in liver metastases from colon carcinoma. *J Nucl Med* 1982;23:1133–1137.
5. DiChiro G. Positron emission tomography using [^{18}F]fluorodeoxyglucose in brain tumors: a powerful diagnostic and prognostic tool. *Invest Radiol* 1986;22:360–371.
6. Paul B. Comparison of fluorine-18-2-fluorodeoxyglucose and gallium-67 citrate imaging for detection of lymphoma. *J Nucl Med* 1987;28:288–292.
7. Alavi JB, Alavi A, Chawluk J, et al. Positron emission tomography in patients with glioma: a predictor of prognosis. *Cancer* 1988;62:1074–1078.
8. Kern KA, Brunetti A, Norton JA, et al. Metabolic imaging of human extremity musculoskeletal tumors by PET. *J Nucl Med* 1988;29:181–186.
9. National Cancer Institute. Study of classifications on non-Hodgkin's lymphomas: summary and description of a working formulation for clinical usage. *Cancer* 1982;49:2112–2135.
10. Patlak CS, Blasberg RG, Frenstermacher JD. Graphical evaluation of blood-to-brain transfer constants from multiple-time uptake data. *J Cereb Blood Flow Metab* 1983;3:1–7.
11. Gjedde A, Wienhard K, Heiss W-D, et al. Comparative regional analysis of 2-fluorodeoxyglucose and methylglucose uptake in brain of four stroke patients. With special reference to the regional estimation of the lumped constant. *J Cereb Blood Flow Metab* 1985;5:163–178.
12. Wienhard K, Pawlik G, Herholz K, et al. Estimation of local cerebral glucose utilization by positron emission tomography of [^{18}F]2-fluoro-2-deoxy-D-glucose: a critical appraisal of optimization procedures. *J Cereb Blood Flow Metab* 1985;5:115–125.
13. Reivich M, Alavi A, Wolf A, et al. Glucose metabolic rate kinetic model parameter determination in humans: the lumped constants and rate constants for [^{18}F]fluorodeoxyglucose and [^{11}C]deoxyglucose. *J Cereb Blood Flow Metab* 1985;5:179–192.
14. Hosoba M, Wani H, Toyama H, et al. Automated body contour detection in SPECT: effects on quantitative studies. *J Nucl Med* 1986;27:1184–1191.
15. Butler JJ, Cleary KR. Histologic diagnosis and classifications of Hodgkin's disease and non-Hodgkin's lymphoma. In: Fuller L. ed. *Hodgkin's disease and non-Hodgkin's lymphomas in adults and children.* New York: Raven Press; 1988:3–46.
16. Hoffman EJ, Huang S-Ch, Phelps ME, et al. Quantitation in positron emission computed tomography. 1. Effect of object size. *J Comput Assist Tomogr* 1979;3:299–308.
17. Yanagawa N, Itou Y, Sekiguchi T, et al. Recovery coefficient in PET: effect of ROI size. *Jap J Radiol Technol* 1989;45:1282.
18. Paul R, Johansson R, Kellokumpu-Lehtinen P-L, et al. Tumor localization with ^{18}F-2-fluoro-2-deoxy-D-glucose: comparative autoradiography, glucose 6-phosphatase histochemistry, and histology of renally implanted sarcoma of the rat. *Res Exp Med* 1985;185:87–94.
19. Suolinna E-M, Haaparanta M, Paul R, et al. Metabolism of 2-[18F]fluoro-2-deoxyglucose in tumor-bearing rats: chromatographic and enzymatic studies. *Nucl Med Biol* 1986;13:577–581.
20. Ter-Pogossian MM. Positron emission tomography instrumentation. In: Reivich M. ed. *Positron emission tomography.* New York: Alan R. Liss; 1985:43–61.
21. Gunaskera SW, King LJ, Lavender PJ. The behavior of tracer gallium-67 towards serum proteins. *Clin Chim Acta* 1972;39:401–406.
22. Wong H, Terner UK, English D, et al. The role of transferrin in the in vivo uptake of gallium-67 in a canine tumor. *Int J Nucl Med Biol* 1980;7:9–16.
23. Muranaka A, Ito Y, Hashimoto M, et al. Uptake and excretion of ^{67}Ga-citrate in malignant tumors and normal cells. *Eur J Nucl Med* 1980;5:31–37.